Design of silica coated polyamide fabrics for thermo-regulating textiles

M. G. G. Altamirano, M. G. Abebe, Joseph Lejeune, A. Cayla, B. Maes, J. Odent, J. M. Raquez, C. Campagne, E. Devaux

Received: 22 December 2022 | Revised: 9 March 2023 | Accepted: 8 April 2023

DOI: 10.1002/app.54004

RESEARCH ARTICLE

Applied Polymer SCIENCE WILEY

Design of silica coated polyamide fabrics for thermo-regulating textiles

M. G. Garzon Altamirano[1,2] | M. G. Abebe[3] | J. Lejeune[2] | A. Cayla[2] | B. Maes[3] | J. Odent[1] | J. M. Raquez[1] | C. Campagne[2] | E. Devaux[2]

[1]Laboratory of Polymeric and Composite Materials (LPCM), Center of Innovation and Research in Materials and Polymers (CIRMAP), University of Mons (UMONS), Mons, Belgium

[2]École Nationale Supérieure Des Arts Et Industries Textiles, Université de Lille, Lille, France

[3]Micro- and Nanophotonic Materials Group, Research Institute for Materials Science and Engineering, University of Mons, Mons, Belgium

Correspondence
J. Lejeune, École Nationale Supérieure Des Arts Et Industries Textiles, Université de Lille, ULR 2461 – GEMTEX – Génie et Matériaux Textiles, Lille F-59000, France.
Email: joseph.lejeune@ensait.fr

Funding information
Interreg Vlaanderen-Nederland

Abstract

Efficient thermal management is essential for the energy balance and thermal comfort. In this context, the design of textiles, which can modulate the infrared radiation emitted by the human body, is attractive. These fabrics will manage the microclimate between the skin and fabric. The proposed textile design consists of the coating of commercial woven fabrics based on polyamide 6–6 by a dip-coating process. The coating is based on the incorporation of fine spherical silica particles with a submicron size within thermosensitive poly(N-isopropylacrylamide) hydrogels. Neat commercial fabrics reflect 12% of the radiation, while the addition of silica particles leads to a reflection of 24% of the infrared radiation in the 5–15 μm wavelengths range. The infrared radiation reflection capacity of the coated fabrics can be increased by managing the size and the content of the silica particles, which allows reaching 36% of reflected radiation. Our findings open opportunities for warming up fabrics and thus reduce energy consumption in heating close space.

KEYWORDS

dip-coating, infrared reflection, personal thermal management, radiative heating, SiO_2 coating

1 | INTRODUCTION

Controlling thermal comfort to maintain the body temperature in a comfortable range (36.5–37.5°C)[1,2] is important to avoid health problems such as hyperthermia, hypothermia, and heat stroke.[2,3] The strategy to manage the thermal comfort of the human body indoors is based on the installation of heating, ventilation, and air conditioning (HVAC) systems. This type of system leads to considerable energy waste and contributes significantly to the energy crisis and global warming.[4,5] Therefore, the dynamic control of the microclimate between the skin and the textile could reduce the energy demand by the HVAC systems.[6] Textiles are a tool for maintaining thermal comfort between the human body and its environment. When the outside temperature is below the comfort temperature, textiles fabrics are supposed to keep the heat in and maintain the temperature. At higher temperatures, textiles fabrics have to dissipate heat from the human body. Energy in the form of heat is evacuated by radiation, convection, evaporation, and conduction, which account for around 60%, 15%, 20%, and 5%, respectively.[7–9] The human body

emits infrared radiation (IR) in the wavelength range between 5 and 15 μm[10–12] with the maximum emission length being around 9 μm.[13]

Conventional clothes have a little interaction in this wavelength radiation range (i.e., 5–15 μm). Therefore, new textile technologies to interact with the human body IR were developed.[14–16] Among the techniques are the use of near-infrared (NIR) reflecting dyes or pigments which color textiles to match reflectance curves, or the "chlorophyll enhancement" of vegetation in the NIR range for camouflage applications.[16,17] Also, the use of dyes made of inorganic micro- or nano-particles during the extrusion process of polyethylene (PE) fibers generates colored PE nanocomposite fabrics and textiles that exhibit around 80% IR transparency.[18] Textile coating allows modulation of IR by incorporating metallic materials, conductive powders, organic/inorganic materials and semi-conductors.[19,20] Among those materials are zinc oxide,[21,22] antimony,[20] carbon nanotubes,[7] silver particles,[9,23–25] silica (SiO_2) particles,[19,26–35] titanium oxide (TiO_2),[27,28] and others.[36,37]

The application of silica as silica oxide or Janus particles (SiO_2-TiO_2) has promising results for personal indoor heating and can also be implemented for the manufacture of conventional textiles. Assaf et al. showed that 5% of submetric SiO_2 particles inserted within PE membranes offer an efficient absorption of more than 35% of the infrared radiation between 5 and 15 μm of the nanocomposite, as compared to the neat membrane.[26] The coating of cotton, wool, viscose, acrylic, and cotton/polyester fabrics with different ceramic powder coatings such as SiO_2 for IR emissivity tuning and management has been studied by Yuce et al.[28] demonstrating the efficient change of IR absorbance in the investigated wavelength range (8–14 μm). Likewise, Panwar et al.[29] deposited Janus TiO_2-SiO_2 particles on a cotton fabric surface and observed a clear NIR reflection due to the coupling of the high refractive index of TiO_2 to the large size of SiO_2 particles.

The application of SiO_2 in textiles has been carried out using different methods, such as SiO_2 aerosol,[38] charges on electrospun fibers,[19] and spray coating.[35] Silica particles have also been applied by co-sedimentation self-assembly as photonic crystals reflecting radiation in the ultraviolet–visible range and coloring fabric substrates.[27] Photonic crystals are periodic structures,[27,38-41] which have the ability to control the propagation of electromagnetic waves in specific wavelength ranges due to the existence of a photonic forbidden band. Following Bragg's law,[42-44] the wavelength at which radiation is reflected depends on the distance between the diffraction planes and the refractive index of the periodical structure. Consequently, silica is a widely used material in optical coatings operating from the ultraviolet (UV) to the NIR. Especially in the NIR range for thermoregulation applications, silica particles are of special interest because they show a reflection peak around 9 μm (i.e., 1110 cm^{-1}). At this wavelength, the human body has its maximum emission of infrared radiation (human body maximum is around 9.8 μm according to a black body emission). Therefore, it is a promising filler for this field.

In the frame of this research, we propose to design smart textiles that reflect the infrared radiation emitted by the human body in the range of 5–15 μm. The textile matrix for the construction of this fabric will be based on woven fibers of PA6-6. This type of textile transmits the IR radiation emitted by the human body[15] and the objective is to transform its properties, allowing reflection of this radiation by the addition of silica particles at the textile surface. The coating process of the textile material will be carried out by a dip-coating process. The coating material will be a thermoresponsive poly(N-isopropylacrylamide) copolymerized with acrylic acid (i.e., P(NIPAM-co-AA)) loaded with silica particles. This thermosensitive polymer will act as a ligand between the particles and the textile. The coating process is completed by free radical photopolymerization of the coating on the textile surface. The influence of the immersion time during the coating process on the reflection of the infrared radiation of the PA6-6/P(NIPAM-co-AA)/SiO_2 coated textiles will be investigated first. Then, the effect of SiO_2 particle concentration will be investigated. Different sizes of silica particles will also be investigated to know how this affects the IR refection of the coated textiles. The use of thermography will also demonstrate the reflective properties of the coated textile. This IR reflective behavior will be correlated with theoretical modeling. This research work changes the properties of a conventional textile by increasing its ability to reflect infrared radiation and thus maintaining body heat and thermal comfort.

2 | MATERIALS, METHODS AND CHARACTERIZATION

2.1 | Materials

N-isopropylacrylamide (NIPAM, 97%, Sigma-Aldrich), acrylic acid (AA, 99.5%, Sigma-Aldrich). N,N-methylenebisacrylamide (MBA, 99%, Sigma–Aldrich), diphenyl (2,4,6-trimethylbenzoyl) phosphine oxide (TPO, 97%, Sigma–Aldrich), deionized water was obtained with a Milli-Q system (Millipore and methanol (99.8%, VWR) were used without further purification. Monodispersed spherical silica particles of 100, 150, and 200 nm of diameter (Fuji Chemical, Silibol 100) were used in powder form. The

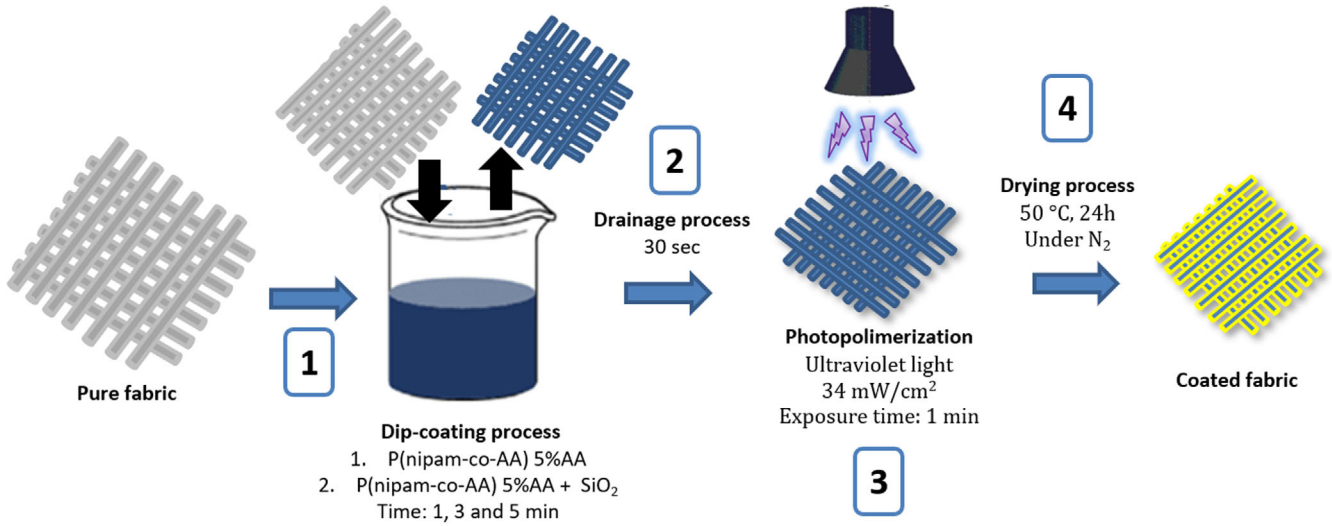

FIGURE 1 Scheme of the coating process. Different steps of the process and parameters for each. (1) Dip-coating: coating material and immersion time. (2) Drainage process. (3) Photopolymerization. (4) Drying process. [Color figure can be viewed at wileyonlinelibrary.com]

density of the silica particles was 2.21 g/cm^3). Commercial polyamide 6–6 woven fabric (thickness: 0.14 mm, areal density: 80 g/m^2) was donated to the GEMTEX laboratory.

2.2 | Preparation of coating dispersion

A thermosensitive P(NIPAM-co-AA)-based coating dispersion was prepared using the MBA as crosslinker and TPO as an initiator in the presence of submicron-sized spherical silica particles of a uniform size. For this purpose, 50 g of NIPAM, 1.36 g of MBA (2 mol%), 1.59 g of AA (5 mol%), and various amounts (between 0 and 50 wt %) of silica were dissolved in 100 mL of methanol: water (75:25 vol%) mixture. Finally, 0.77 g of TPO (0.5 mol%) is added to the mixture. The initiator enables free radical photopolymerization of the acrylate groups after the dip coating process.[45]

2.3 | Dip-coating process

The pure PA6-6 fabric, named (F), was immersed in the solution of the coating material (P(NIPAM-co-AA)), identified as (P), and (P) + SiO_2 particles. (F) remained in the solution for a given time (1, 3, or 5 min). After the immersion time had ended, the excess liquid was drained from the surface by gravity (30 s). The thermosensitive coating was adhered to the fabric by free radical photopolymerization by near UV exposure (34 mW/cm^2) for 1 min of the wet fabric. The solvent methanol: water was evaporated in the drying step at 50°C under vacuum for 24 h forming the thin layer on the fabric surface (as explained in Figure 1). The coated samples were stored at ambient conditions 20°C and 60% relative humidity.

2.4 | Characterization

2.4.1 | Areal density

The 9 cm^2 samples were weighed after the coating process at the end of the drying stage. The areal density using Equation 1 is calculated as the average of three samples.

$$\text{Areal density}\left(g/m^2\right) = \frac{\text{Dry fabric weight}\,(g)}{\text{Dry fabric area}\,(m^2)} \quad (1)$$

2.4.2 | Thickness measurement

For the determination of the fabric thickness before and after the coating process, a digital caliper 0–150 mm FOWLER (Tools and Instruments) was used, and every value presented (in mm) is averaged over 10 separate measurements.

2.4.3 | Thermogravimetry

Thermogravimetry (TGA) of fabric samples was evaluated by TGA Q500, TA Instruments. The fabric samples before and after the coating process were analyzed

(10–15 mg) over the temperature range of 25–800°C at a heating rate of 10°C/min under nitrogen (N_2) atmosphere.

2.4.4 | Fourier transform infrared spectroscopy

A Shimadzu IR Prestige-21 spectrometer equipped with an integrating sphere was used. The fabrics samples (stored at 20°C and 60% RH) were analyzed in reflectance mode in a wide range from 2 μm (5000 cm^{-1}) to 28 μm (350 cm^{-1}) by 64 scans. The experimental data were collected and analyzed using the Varian Resolutions Pro software.

2.4.5 | Scanning electron microscopy

A Hitachi SU8020 device at a voltage of 5 kV was used to obtain the coating thickness (cross section) and to check the size of SiO_2 particles in the coating layer (surface). The coated fabrics stored at 20°C and 60% RH were cut into small pieces. The resulting samples were coated with a thin layer of carbon as a conductive material to facilitate analysis.

2.4.6 | Thermal measurement

A type K thermocouple (TK2000 Chauvin-Arnoux) measuring temperature ranges from −40 to +200°C were used on the surface of the skin. The coated fabric (9 cm^2) was placed on top of the thermocouple and the temperature was measured in the microclimate generated between the skin and the coated fabric. All samples were held for 30 s on the skin to achieve thermal equilibrium before taking the system temperature measured. During all measurements, the ambient temperature was maintained at ∼20°C and the relative humidity was kept at ∼60%. The images were analyzed using ImageJ software for processing and analyzing scientific images.

2.4.7 | Thermal imaging

A FLIR C2 compact professional thermal imaging camera was used. This 80 × 60 pixels camera records infrared radiation in a spectral range of 7.5–14 μm and temperature ranges of −10–150°C with an image upgrade rate of 9 Hz. The protocol followed for the analysis of the samples was to keep them under constant humidity and temperature conditions (60% RH at 20°C). All samples were kept for 30 s on the skin to get the thermal equilibrium prior to imaging. Finally, the images were captured at a fixed distance of 12 cm.

2.4.8 | Theoretical model

To study the IR reflection of the engineered materials theoretically: in one case, the collision-based Monte Carlo method for solving the radiative transfer through the sample was implemented. In another case, the finite element method to calculate rigorous solutions of Maxwell's equations using commercial software was utilized (COMSOL Multiphysics® v5.3).

3 | RESULTS

This study proposes to design smart textiles that are able to modulate the infrared radiation emitted by the human body in the wavelengths range of 5–15 μm. For this purpose, thermosensitive hydrogels incorporating silica particles capable of modulating the reflection of infrared radiation were applied as a coating on commercial PA6-6 fabrics (F). A thin coating layer of ca. 20–65 μm was obtained by a dip-coating process and free radical photopolymerization of thermosensitive N-isopropylacrylamide (NIPAM) and acrylic acid (AA) in the presence of N,N′-methylenebisacrylamide (MBA) as crosslinker. Therein, diphenyl(2,4,6-trimethylbenzoyl) phosphine oxide (TPO), a type I photoinitiator, allows free radical photopolymerization of the acrylate groups within 1 min under near UV exposure. The fine silica particles dispersed within the hydrogel matrix spontaneously form colloidal particle arrays in a non-packed state. Thus, this coating should efficiently diffract light, complying with the Bragg condition, which is determined by the spacing between the diffracting planes of the colloidal crystals.[46]

As far as the dip-coating process is concerned, the fabrics were immersed for 1, 3, and 5 min in the coating solutions made of neat P(NIPAM-co-AA) or P(NIPAM-co-AA) + 20 wt% SiO_2. After the stages of the coating process: drainage (30 s), photopolymerization (1 min) and drying, the effect of the coating layer was studied by analyzing the textile properties, morphology, and reflection of infrared radiation. TGA, FTIR, Scanning Electron Microscopy (SEM), and thermal measurement, and imaging by IR camera were used to analyze three different effects: immersion time, SiO_2 content (wt%), and SiO_2 size in the coating solution.

The areal density of the woven fabric PA6-6 was determined as 80 g/m^2. After coating depending on the immersion time, the areal density increases to 124.8

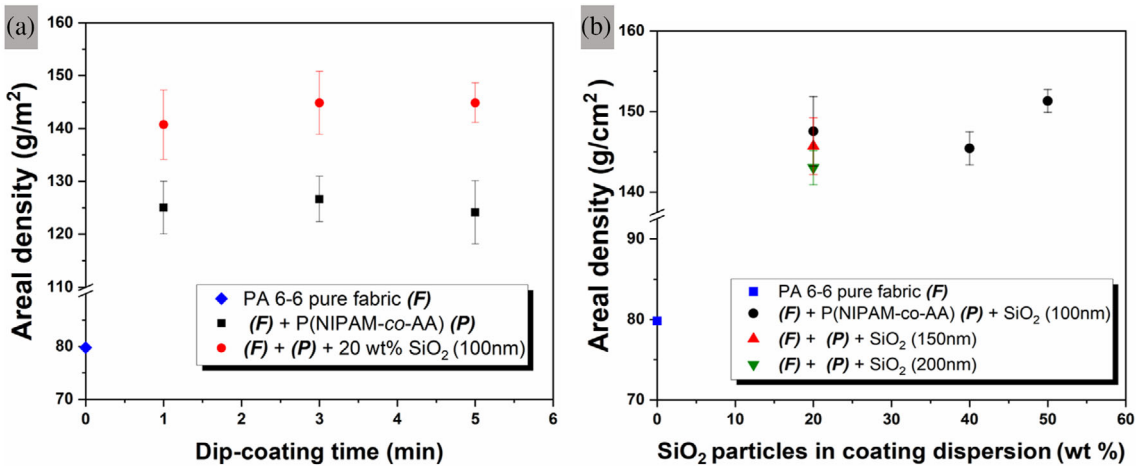

FIGURE 2 Analysis of the properties of PA6-6 fabrics after the coating process. (a) Evolution of the areal density in fabrics coated with (P) and (P) + 20 wt% SiO_2 (100 nm) as a function of the immersion time in the dip-coating stage. (b) Evolution of the areal density in the fabrics coated with (P) + SiO_2 particles analyzing the effect of the amount (wt%) and size of SiO_2 particles in the coating dispersion (constant dip-coating time 3 min). [Color figure can be viewed at wileyonlinelibrary.com]

TABLE 1 Thermogravimetric analysis of coated fabrics to obtain the final wt% of SiO_2 particles after the coating process. The amount of SiO_2 is determined as a result of the analysis of the residue at 800°C.

Sample	% residue at 800°C	
(F)	2.4 ± 0.1	
(F) + (P) (3 min)	2.4 ± 0.2	
Sample	**% Residue at 800°C**	**% SiO_2**
(F) + (P) + 20 wt% SiO_2 (100 nm)	15.8 ± 0.4	13.4 ± 0.4
(F) + (P) + 40 wt% SiO_2 (100 nm)	18.9 ± 0.6	16.5 ± 0.6
(F) + (P) + 50 wt% SiO_2 (100 nm)	26.1 ± 0.3	23.7 ± 0.3
(F) + (P) + 20 wt% SiO_2 (100 nm)	15.8 ± 0.4	13.4 ± 0.4
(F) + (P) + 20 wt% SiO_2 (150 nm)	16.9 ± 0.2	14.5 ± 0.2
(F) + (P) + 20 wt% SiO_2 (210 nm)	16.6 ± 0.3	14.2 ± 0.3

± 0.4 g/m^2 for the (F) + (P) and 143.2 ± 0.8 g/m^2 for (F) + (P) + 20 wt% SiO_2 (100 nm) (Figure 2a). Keeping the immersion time constant at 3 min, the areal density increases to (151.2 ± 0.8) g/m^2 of (F) + (P) + SiO_2 based on SiO_2 content (20–50 wt%) and to (146.1 ± 1.5) g/m2 of (F) + (P) + SiO_2 based on SiO_2 size (100–200 nm) in the coating solution (Figure 2b). The size of the particles changed in these second pictures, but the weight percentage remained constant. Therefore, the areal density remained almost constant. The thickness of the coated fabrics was also analyzed and remains between 0.16 and 0.18 mm in all cases (Table S1 and Figure S1 in the ESI). The areal density enables the classification of the textile fabric as a light fabric (below 100 g/m^2) a medium fabric (between 100 and 200 g/m^2) and a heavy fabric (over 200 g/m^2). The coating changed the classification of the fabric but is still in the range of used fabric in clothing applications.

Thermogravimetric analysis was carried out to analyze the commercial reference fabric (F) and the SiO_2 coated fabrics to determine the amount of silica particles in the coated fabrics. The results showed (F) an inorganic residue of 2.4% at 800°C. From this result, the SiO_2 content of the coated fabrics was calculated as the difference between the residue of neat fabric and coated fabric (Table 1). The percentage of SiO_2 in the fabrics after the coating process is lower than the SiO_2 content in the coating solutions. Moreover, the deposited quantity of SiO_2 does not increase proportionally to the SiO_2 content in the solutions, and could be related to a lack of affinity between SiO_2 particles and fabrics as shown by the results obtained. The size of the particles seems in the presented tests to have a low effect on the deposited quantity (Table 1). Indeed, the particles count decreased but the deposited weight percent remained constant which is also supported by areal density measurements.

To demonstrate the effect of the coating based on a thermosensitive polymer and silica particles on IR reflection in the framework of body thermoregulation, the study focused on the characterization of the mid-infrared range (5–15 μm) (Figure 3). The coating time was varied between the (P) and (P) + SiO_2 based coating. The

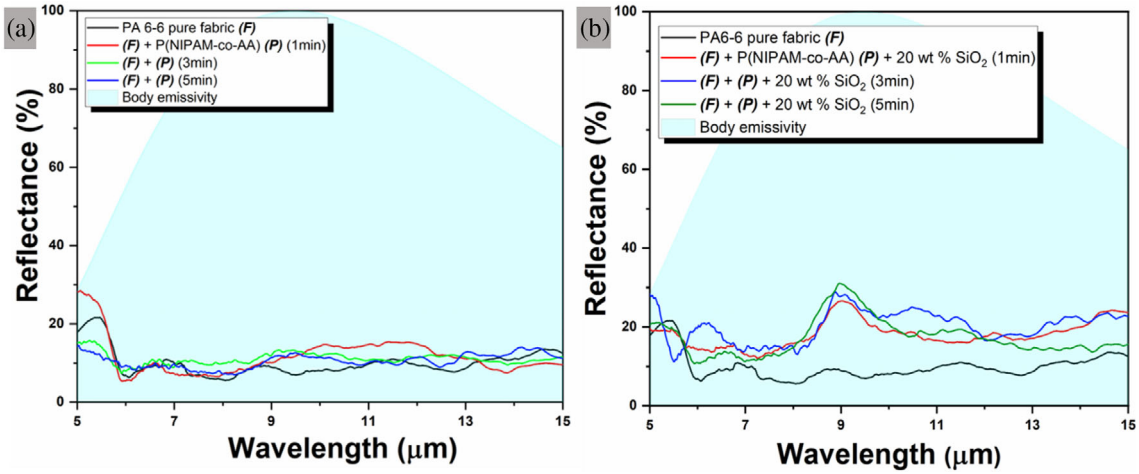

FIGURE 3 Evolution of the infrared spectral curves in the 5–15 μm range of the coated fabric as a function of increasing immersion time between 1 and 5 min at 20°C and 60% relative humidity. The blue area indicates the spectral emissivity by the human body. (a) Infrared spectral curves of PA6-6 coated by (P). (b) Infrared spectral curves of PA6-6 coated by (P) + 20 wt% SiO_2 (100 nm). [Color figure can be viewed at wileyonlinelibrary.com]

reference spectral curve is the pure PA6-6 fabric (Figure 3a-black solid line). The coating of only thermo-sensitive polymer (P) does not affect the intensity of the spectral curves (Figure 3a). However, in all spectral curves, a variation in IR reflection is observed between 5 and 7 μm. This reflection zone could be due to the backscattering of some photons (electromagnetic waves) inside the structure.[47] When monodispersed silica particles were included in the coating solution, the spectral curves increased in intensity affected by the presence of SiO_2 (Figure 3b). As in the case of the thermosensitive polymer coating, a first zone of reflection changes was observed between 5 and 7 μm. In addition, a second reflection peak at 9.2 μm was observed, the intensity of which depends directly on the presence of SiO_2 particles.[46-48] The intensity of this zone for the pure fabric reached only 10% IR reflection, while the maximum intensity of the peak related to the presence of silica is 36% IR reflection for the fabrics coated with (P) + 20 wt% 100 nm SiO_2 for 5 min. The behavior of IR reflection on coated fabrics is affected by the amount and distribution of SiO_2 particles within the coating layer.[46,49]

After obtaining the infrared radiation reflection spectra, $\rho(\%)$ was determined as a standard measure of the amount of infrared radiation emitted by the human body that is reflected by the coated fabrics. $\rho(\%)$ is given by Equation 2[50,51]:

$$\rho(\%) = \frac{\int_{\lambda_1}^{\lambda_2} R(\lambda)\, \emptyset_{bb}(\lambda) d\lambda}{\int_{\lambda_1}^{\lambda_2} \emptyset_{bb}(\lambda) d\lambda} \times 100 \qquad (2)$$

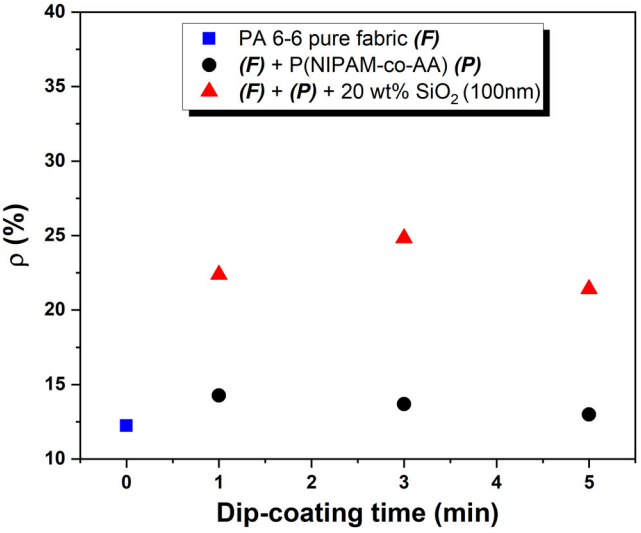

FIGURE 4 Percentage of reflected infrared radiation emitted by the human body at 34°C between 5 and 15 μm (ρ). Samples analyzed as a function of increasing immersion time between 1 and 5 min at 20°C and 60% RH. Samples: PA6-6 pure fabric (F) (square symbol – reference), PA6-6 coated by P(NIPAM-co-AA) (P) (round symbol), and PA6-6 coated by (P) + 20 wt% SiO_2 (100 nm) (triangular symbol). [Color figure can be viewed at wileyonlinelibrary.com]

where R(λ) is the reflection spectrum of the fabric (Table S2 in the ESI), $Ø_{bb}$ is Planck's black body distribution for a skin temperature at 34°C, and (λ_1, λ_2) is the wavelength interval of the human body thermal emission spectrum (5–15 μm). Figure 4 shows the evolution of $\rho(\%)$ as a function of immersion time. The reference

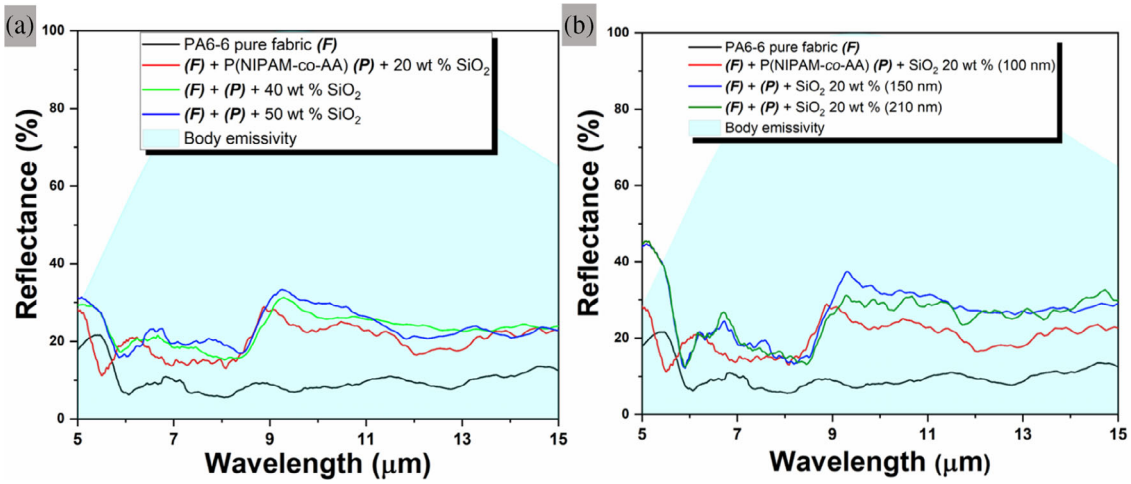

FIGURE 5 Evolution of the infrared spectral curves in the 5-15 μm range of the coated fabric at 20°C and 60% relative humidity. The blue area indicates the spectral emissivity by the human body. (a) Infrared spectral curves of PA6-6 coated by P(NIPAM-co-AA) + 20 wt% SiO_2 (100 nm) analyzing the effect of wt% SiO_2 in the dispersion coating. (b) Infrared spectral curves of PA6-6 coated by P(NIPAM-co-AA) + SiO_2 analyzing the effect of SiO_2 size in dispersion coating. [Color figure can be viewed at wileyonlinelibrary.com]

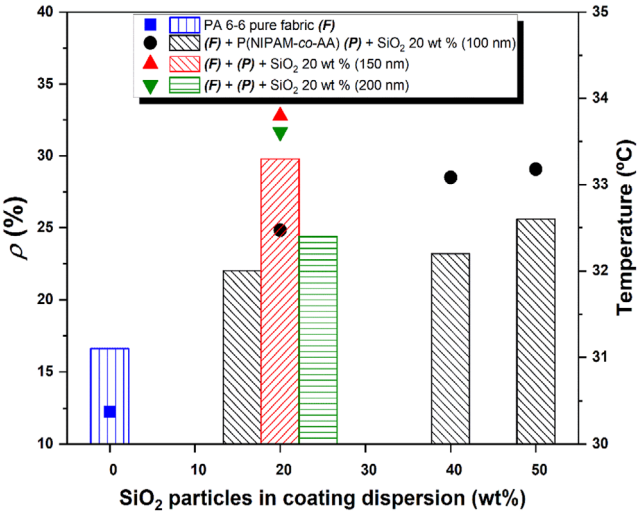

FIGURE 6 Left axis (for symbols): Evolution of percentage of reflected radiation of the infrared radiation emitted by the human body at 34°C between 5 and 15 μm. $\rho(\%)$ at 20°C and 60% RH. Analysis of different effects: wt% and SiO_2 size in the coating dispersion. PA6-6 pure fabric (F) (square symbol – reference). Right axis (bar chart): Variation of the temperature measured by the thermocouple in the space between the skin and the textile according to the effect of wt% and SiO_2 size at 20°C and 60% RH. (Skin temperature: 30.5°C). [Color figure can be viewed at wileyonlinelibrary.com]

fabric PA6-6 reflects 12% of the infrared radiation emitted by the human body in the range 5–15 μm. Using the thermosensitive polymer (P) as a coating at different immersion times, this percentage increased to 14% and remained constant over time. The percentages of IR reflected reached values between 22% and 25% when the coating of the commercial fabrics used (P) + 20 wt% 100 nm SiO_2 at different immersion times between 1 and 5 min (Figure 4). It is observed that the reflection of infrared radiation is increased by the presence of silica particles in the coating and that the immersion time during the coating process has low or no effect on the IR response of the coated fabrics. Therefore, the immersion time of 3 min was used to investigate the effect of SiO_2 content and SiO_2 size in the coating solution.

Subsequently, the influence of the amount of SiO_2 particles on the IR reflection in the range 5–15 μm is investigated. For this purpose, the particle size was kept at 100 nm and the content in the coating solution was varied. The resulting spectral curves show the characteristic peak of silica around 9 μm (Figure 5a). The intensity of this reflection range increases from 25% at 20 wt% to 38% at 50 wt% SiO_2. By applying Equation 2, $\rho(\%)$ is obtain as a function of wt% SiO_2 in the coating solution (Figure 6 round symbol). The reflection percentage increased with the increasing amount of SiO_2 in the coating solution. This increase depends not only on the amount of SiO_2 but also on its distribution and the thickness of the coating layer. By analysis of SEM images using ImageJ software (Figure 6 and Figure S2 in the ESI), it was observed that all wt% SiO_2 coatings showed agglomerations of 0.33 μm, while the distance between these agglomerations and the thickness of the coating layer were determined (Table S2 and Figure S1 in the ESI). The coating layer of the (F) treated with (P) + 20 wt % SiO_2 has ~40 μm and the distance between the particles is ~0.83 μm. By increasing wt% SiO_2 to 50 wt% the thickness coating increases and the distance between the particles decreases to ~65 and 0.38 μm respectively

TABLE 2 Thermal measurements of the PA6-6/P(NIPAM-co-AA)/SiO_2 fabric samples. Analysis of different effects: wt% and size of SiO_2 particles in coating dispersion. Skin and ambient temperatures: 30.5 and 20°C respectively.

Sample	Temperature between skin and fabric (°C)
PA 6–6 pure fabric (F)	31.1
(F) + P(NIPAM-co-AA) (P) (min 3)	31.3
(F) + (P) + 20 wt% SiO_2 (100 nm)	32.0
(F) + (P) + 40 wt% SiO_2 (100 nm)	32.2
(F) + (P) + 50 wt% SiO_2 (100 nm)	32.6
(F) + (P) + 20 wt% SiO_2 (100 nm)	32.0
(F) + (P) + 20 wt% SiO_2 (150 nm)	33.3
(F) + (P) + 20 wt% SiO_2 (210 nm)	32.4

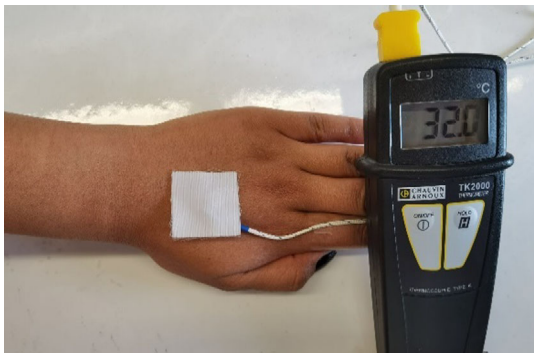

FIGURE 7 Photo of the thermal measurement setup: a thermocouple measuring the microclimate between the skin and coated fabric samples. [Color figure can be viewed at wileyonlinelibrary.com]

(Table S2 in the ESI). Decreasing the spacing between the dispersed particles increases the reflection of the infrared radiation.[52,53] Likewise, increasing the thickness of the coating layer increases the reflection of infrared radiation between 5 and 15 μm.[54,55]

Keeping the SiO_2 content constant at 20 wt%, the particle size on the coating solution was changed to analyze its influence on the IR reflection between 5 and 15 μm. The resulting spectral curves (Figure 5b) show the characteristic peak of SiO_2 around 9 μm and an increase in intensity over the whole wavelength range between 5 and 15 μm with respect to the SiO_2 particle size. By applying Equation 2, the percentage of infrared radiation reflected by the coated fabrics as a function of silica particle size was evaluated (Figure 6). $\rho(\%)$ for (P) + SiO_2 coated fabrics with 100 nm particles is 24%, reaching up 34% with 200 nm SiO_2 and 36% with 150 nm SiO_2. These trends of infrared radiation reflection are related to the morphology of the coating layer and the distribution of the SiO_2 particles. $\rho(\%)$ increases when the distance between the particles decreases, this correlation we observed by morphological analysis.

Then a SEM image analysis of coated fabrics (Figure S2 in the ESI) by ImageJ allowed obtaining the distance between the particles and the size of the agglomerations in the coating layer. The results show (Table S1 in the ESI) SiO_2 particles in the (P) + 20 wt% SiO_2 (100 nm) coated fabrics form agglomerations and the distance between them is ~0.83 μm. In the (P) + 20 wt% SiO_2 (150 nm) and (P) + 20 wt% SiO_2 (200 nm) coated fabrics, no agglomerations were observed, only single particles, and the distance between them were 0.44 and 0.63 μm respectively. As the particle size increases from 100 to 150 nm, the thickness decreases slightly, this behavior should decrease the IR reflection, however the influence of the particle distribution is stronger, producing the opposite effect and increasing $\rho(\%)$ from 24% to 36%. At larger particle size (200 nm), the coating thickness is practically constant, and the reflection of infrared radiation decreases slightly due to the increase in the distance between the particles.

Thermal analysis was carried out to evaluate the thermal efficiency of the coated fabrics by using a thermocouple between the coated fabric and the skin. The skin temperature was measured by the thermocouple (30.5 ± 0.5°C). The temperatures registered (Table 2) by the thermocouple showed that (F) can slightly increase the skin surface temperature. The neat fabrics reflected 12% of IR, no major effect is observed because PA6-6 is characterized by the transmission of infrared radiation. In samples coated by (P), the surface temperature increases up to 31.3°C creating a slight heating effect on the skin.[25] When SiO_2 particles are introduced into the fabric coating, regardless of their content or size, the temperature of the microclimate between the fabric and the skin increases. This increase is directly related to the percentage of reflected infrared radiation (Figure 6). A larger $\rho(\%)$ means a higher temperature at the skin surface, as shown by the results of the (F) + (P) + 20 wt% SiO_2 (150 nm) coated fabrics whose $\rho(\%)$ is 36% and the temperature is 33.3°C. These results demonstrate a warming effect on the body surface, maintaining the thermal comfort in an assumed outdoor scenario with cold ambient temperatures (Figure 7).

Infrared thermography allows the reflection of infrared radiation from coated woven textiles to be analyzed, providing the apparent surface temperature of the materials (Table S4 in the ESI). The results obtained from infrared thermal imaging are in coherence with previous trends (Figure 8). The lower the temperature between the

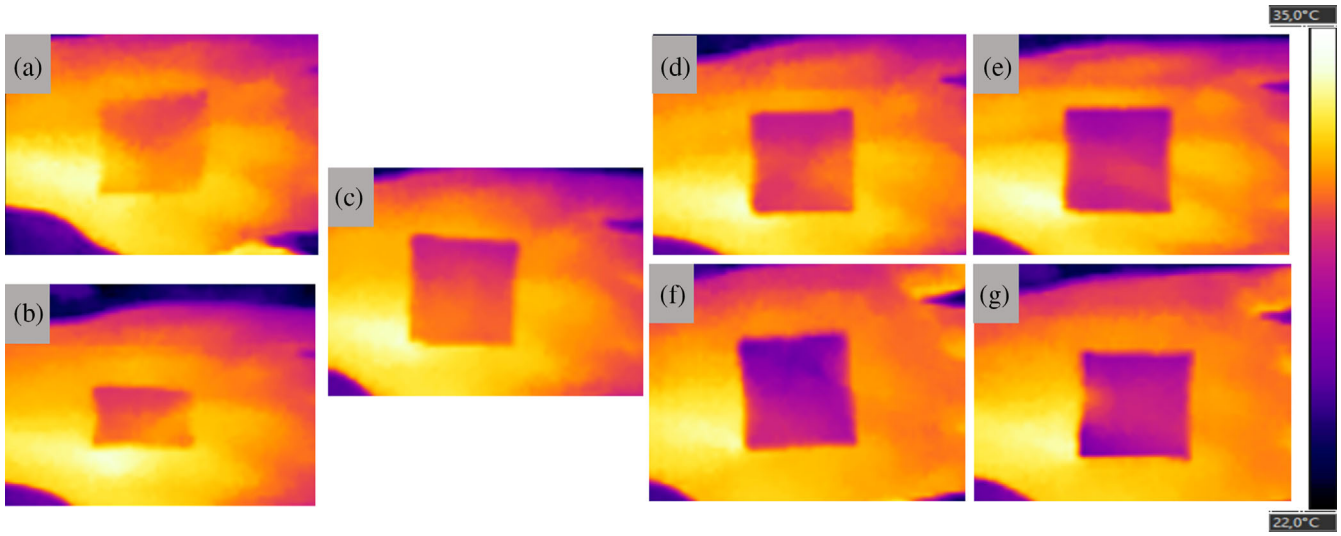

FIGURE 8 Infrared images of the hand covered with the (a) PA 6–6 pure fabric (F), (b) (F) coated by P(NIPAM-co-AA) (P), (c) (F) + (P) + 20 wt% SiO_2 (100 nm) (d) (F) + (P) + 40 wt% SiO_2 (100 nm) (e) (F) + (P) + 50 wt% SiO_2 (100 nm) (F) (F) + (P) + 20 wt% SiO_2 (150 nm) (g) (F) + (P) + 20 wt% SiO_2 (200 nm). [Color figure can be viewed at wileyonlinelibrary.com]

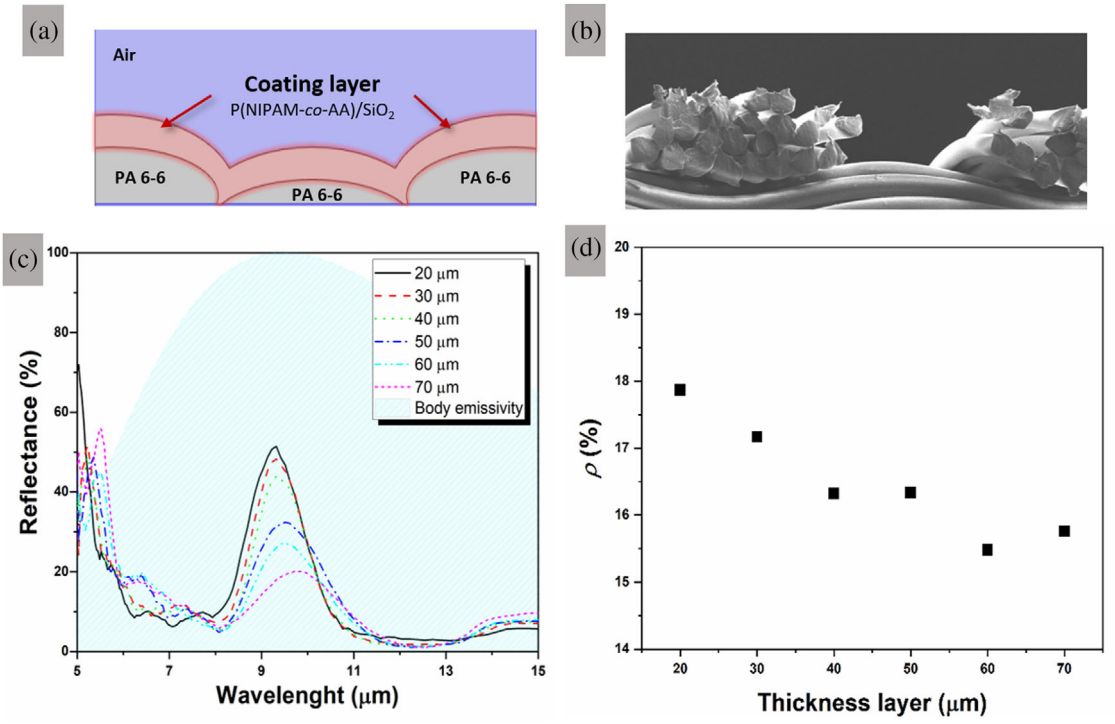

FIGURE 9 Theoretical model obtained from the experimental results to support the different behavior of the coated fabrics with infrared radiation in the range of 5–15 μm. (a) Schematic of the designed periodic structure with the real dimensions of the fabrics. (b) SEM cross section view of the commercial PA6-6 fabric structure. (c) Reflection spectra of the coated fabrics as a function of the thickness of the (F) + (P) + SiO_2 (100 nm) **2**0 wt% coating layer. (d) Evolution of the percentage of reflected infrared radiation (ρ) between 5 and 15 μm as the coating thickness changes. [Color figure can be viewed at wileyonlinelibrary.com]

fabric and the skin, the more energy the fabric radiates because infrared radiation is being transmitted as in the case of pure fabric (Figure 8a). Thermal images of "warm" apparent temperatures indicate high emittance in the IR range, which means that some of the infrared radiation emitted by the human body is being lost to the environment, thereby increasing the temperature of the outer surface of the fabric (Figure 8b). In contrast, the IR camera showed "cooler" apparent temperature in (P) + SiO_2 coated fabrics (Figure 8c), indicating that less IR

is being released from the human body. This is because the tissue is reflecting this radiation and creating a heating effect between the coated fabric and the skin.

3.1 | Theoretical model

A theoretical model was designed to support the infrared radiation reflection profile in the 5–15 μm range of the treated fabrics as a function of coating thickness. For the realization of the theoretical model, it was necessary to design a periodic structure (Figure 9a) based on the real fabric. (Figure 9b). Likewise, it was assumed that the coating consists of a hydrogel matrix considered as an ideal polymer whose refractive index is set at 1.5 as an approximate value for PNIPAM-based materials.[56,57] As for the silica particles, their size and wt% were set to 100 nm and 20% respectively. Furthermore, the particles were assumed to be homogeneous and well dispersed within the surface layer made by the hydrogel. Simulation is done by finite element method using COMSOL to obtain the reflection spectra. Figure 9c shows the reflection peak at 9 μm, stemming from the silica material strong phonon-polariton resonance.[58,59] At this wavelength, silica has a large extinction coefficient (k), hence a negative permittivity. The maximum intensity of this peak is 50% with a 20 μm thick layer. As the thickness increases the intensity, position, and shape of this peak changes resulting in a decrease in intensity, a lateral shift to a longer wavelength and an increase in the width of the reflection peak. These changes are due to an increase in the absorption of infrared radiation at 10 μm (Figure S3 in the ESI). As the thickness of the coating layer increases, the depth of wrinkles on the surface decreases, therefore, a flat surface could be achieved, which could cause the reflection to increase.[54]

However, a higher thickness also means more material creating the wrinkles, and this leads to an increase in infrared absorption.[60] Thus, the opposite effect occurs and the reflection of infrared radiation decreases. As shown in Figure 9d, once the integration method has been applied (Table S5 in the ESI), the theoretical percentage of infrared radiation reflected (ρ) by the coated fabrics is obtained, thereby proving that as the thickness layer increases, the reflection decreases and the absorption of infrared radiation increases.

4 | CONCLUSIONS

A textile capable of modulating the infrared radiation emitted by the human body in the range of 5–15 μm was successfully developed. The materials are based on PA6-6 as the textile matrix and thermosensitive PNIPAM-based polymers loaded with SiO_2 particles as a coating. The coating process was carried out in several stages, the most important being the immersion stage and the photopolymerization stage to impregnate the textile with the coating solution and to fix the coating, respectively. In order to study the efficiency of the coating on the infrared radiation reflection, different effects were analyzed: immersion time during the coating process and content and size of the coating solution. The results obtained show that the presence of SiO_2 particles in the coating increases the percentage of infrared radiation reflected by the coated material, doubling the percentage of reflection of the pure material. It was also shown that this percentage of reflection is influenced by the size and distribution of the particles as well as by the thickness of the coating layer. The fabric coated with P(NIPAM-co-AA) + 20 wt% SiO_2 (150 nm) was the most efficient, reflecting 36% of the infrared radiation emitted by the human body. This result was confirmed by thermal analysis of the textiles indicating an increase in temperature between the textile and the skin. Therefore, the developed (P) + SiO_2 fabrics are expected to be used in warming up textile applications.

AUTHOR CONTRIBUTIONS

M. G. Garzon Altamirano: Conceptualization (supporting); data curation (lead); formal analysis (equal); writing – original draft (lead); writing – review and editing (equal). **M. G. Abebe:** Software (equal); validation (supporting); writing – original draft (supporting); writing – review and editing (supporting). **J. Lejeune:** Conceptualization (equal); methodology (equal); supervision (lead); validation (lead); writing – original draft (equal); writing – review and editing (lead). **A. Cayla:** Conceptualization (equal); supervision (equal); validation (lead); writing – review and editing (equal). **B. Maes:** Validation (supporting); writing – review and editing (supporting). **J. Odent:** Conceptualization (equal); supervision (lead); validation (equal); writing – review and editing (equal). **J. M. Raquez:** Conceptualization (equal); funding acquisition (lead); supervision (equal); validation (equal). **C. Campagne:** Supervision (supporting); writing – review and editing (supporting). **E. Devaux:** Funding acquisition (lead); supervision (supporting); writing – review and editing (supporting).

ACKNOWLEDGMENTS

The authors disclosed receipt of the following financial support for the research, authorship, and/or publication of this article by Interreg France-Wallonie-Vlaanderen program, under the PHOTONITEX project. Jean-Marie Raquez is an FRS-FNRS senior scientific researcher.

CONFLICT OF INTEREST STATEMENT

The authors declare no conflicts of interest.

DATA AVAILABILITY STATEMENT

The data that support the findings of this study are available from the corresponding author upon reasonable request.

ORCID

M. G. Abebe https://orcid.org/0000-0002-7284-5710
J. Lejeune https://orcid.org/0000-0001-9090-3403
A. Cayla https://orcid.org/0000-0001-5031-3396
B. Maes https://orcid.org/0000-0003-3935-7990
J. Odent https://orcid.org/0000-0002-3038-846X
J. M. Raquez https://orcid.org/0000-0003-1940-7129
C. Campagne https://orcid.org/0000-0001-5223-0236
E. Devaux https://orcid.org/0000-0003-0850-138X

REFERENCES

[1] K. Min, Y. Son, C. Kim, Y. Lee, K. Hong, *Int. J. Heat Mass Tran.* **2007**, *50*, 5292.
[2] H. M. K. Ullah, J. Lejeune, A. Cayla, M. Monceaux, C. Campagne, É. Devaux, *Text. Res. J.* **2021**, *92*, 3351.
[3] J. González-Alonso, *Exp. Physiol.* **2012**, *97*, 340.
[4] G. Walther et al., *Nature* **2002**, *416*, 389.
[5] N. Oreskes, *Science* **2005**, *306*, 2004.
[6] C. Liu et al., *Nat. Commun.* **2017**, *8*, 496.
[7] X. A. Zhang, S. Yu, B. Xu, M. Li, Z. Peng, Y. Wang, S. Deng, X. Wu, Z. Wu, M. Ouyang, Y. H. Wang, *Science* **2019**, *363*, 619.
[8] Y. Zhai, Y. Ma, S. N. David, D. Zhao, R. Lou, G. Tan, R. Yang, X. Yin, *Science* **2017**, *355*, 1062.
[9] X. Yue, T. Zhang, D. Yang, F. Qiu, Z. Li, G. Wei, Y. Qiao, *J. Colloid Interface Sci.* **2019**, *535*, 363.
[10] W. Bierman, *J. Am. Med. Assoc.* **1936**, *106*, 1158.
[11] K. Witek, T. Piotrowski, A. Skwarek, *Mater. Sci. Eng. B* **2012**, *177*, 1373.
[12] S. W. Lee, C. H. Lim, E. I. B. Salleh, *Renew. Sustain. Energy Rev.* **2016**, *65*, 643.
[13] Y. Shabany. 1Chapter 3 Radiation Heat Transfer. **2020**.
[14] H. Liu, C. Wang, G. Chen, Y. Liao, M. Mao, T. Cheng, A. Libanori, X. Xiao, X. Hu, K. Liu, J. Chen, *Nano Energy* **2022**, *93*, 106855.
[15] R. Xiao, C. Hou, W. Yang, Y. Su, Y. Li, Q. Zhang, P. Gao, H. Wang, *ACS Appl. Mater. Interfaces* **2019**, *11*, 44673.
[16] L. M. Degenstein, D. Sameoto, J. D. Hogan, A. Asad, P. I. Dolez, *Micromachines* **2021**, *12*, 773.
[17] D. Stokols, I. Altman, J. Wiley, *Handbook of Technical Textiles*. Woodhead Publishing, Ltd, Cambridge **1987**.
[18] T. Kim, S. Jeon, D. Kwak, Y. Chae, *Fibers Polym.* **2012**, *13*, 212.
[19] K. Qiu, A. Elhassan, T. Tian, X. Yin, J. Yu, Z. Li, B. Ding, *ACS Appl. Mater. Interfaces* **2020**, *12*, 11016.
[20] S. M. Jeong, J. Ahn, Y. K. Choi, T. Lim, K. Seo, T. Hong, G. H. Choi, H. Kim, B. W. Lee, S. Y. Park, S. Ju, *NPG Asia Mater.* **2020**, *12*, 32.
[21] S. Fang, W. Wang, X. Yu, H. Xu, Y. Zhong, X. Sui, L. Zhang, Z. Mao, *Mater. Lett.* **2015**, *143*, 120.
[22] L. Cai, A. Y. Song, W. Li, P. C. Hsu, D. Lin, P. B. Catrysse, Y. Liu, Y. Peng, J. Chen, H. Wang, J. Xu, A. Yang, S. Fan, Y. Cui, *Adv. Mater.* **2018**, *30*, 1802152.
[23] Z. Yang, H. Peng, W. Wang, T. Liu, *J. Appl. Polym. Sci.* **2010**, *116*, 2658.
[24] P. C. Hsu, X. Liu, C. Liu, X. Xie, H. R. Lee, A. J. Welch, T. Zhao, Y. Cui, *Nano Lett.* **2015**, *15*, 365.
[25] X. Li, Y. Yang, Z. Quan, L. Wang, D. Ji, F. Li, X. Qin, J. Yu, S. Ramakrishna, *Chem. Eng. J.* **2022**, *430*, 133093.
[26] M. Boutghatin, S. Assaf, Y. Pennec, M. Carette, V. Thomy, A. Akjouj, B. Djafari Rouhani, *Nanomaterials* **2020**, *10*, 1.
[27] Y. Li, L. Zhou, G. Liu, L. Chai, Q. Fan, J. Shao, *Appl. Surf. Sci.* **2018**, *444*, 145.
[28] I. Yuce, S. Canoglu, S. M. Yukseloglu, R. Li Voti, G. Cesarini, C. Sibilia, M. C. Larciprete, *Sensors* **2022**, *22*, 3918.
[29] K. Panwar, M. Jassal, A. K. Agrawal, *Surf. Coatings Technol.* **2017**, *309*, 897.
[30] Z. hui Liu, F. Wang, Z. Ping Deng, *Constr. Build. Mater.* **2016**, *122*, 548.
[31] A. A. Günay, H. Kim, N. Nagarajan, M. Lopez, R. Kantharaj, A. Alsaati, A. Marconnet, A. Lenert, N. Miljkovic, *ACS Appl. Mater. Interfaces* **2018**, *10*, 12603.
[32] H. Liu, S. Li, H. Li, Z. Chen, J. Li, Y. Li, *J. sol-Gel Sci. Technol.* **2018**, *88*, 519.
[33] H. Liu, Y. Xu, C. Tang, Y. Li, N. Chopra, *Ceram. Int.* **2019**, *45*, 23393.
[34] Z. Lu, E. Strobach, N. Chen, N. Ferralis, J. C. Grossman, *Joule* **2020**, *4*, 2693.
[35] X. Zhou, W. Song, G. Zhu, *Cellulose* **2020**, *27*, 2927.
[36] A. Khalili, A. Mottaghitalab, M. Hasanzadeh, V. Mottaghitalab, *Int. J. Ind. Chem.* **2017**, *8*, 109.
[37] S. R. Yousefi, O. Amiri, M. Salavati-Niasari, *Ultrason. Sonochem.* **2019**, *58*, 104619.
[38] L. Lin, Z. Li, H. Mao, W. Li, C. Wang, *Front. Mater.* **2021**, *8*, 1.
[39] J. F. Galisteo-Lõpez, M. Ibisate, R. Sapienza, L. S. Froufe-Pérez, Ú. Blanco, C. Lõpez, *Adv. Mater.* **2011**, *23*, 30.
[40] S. John, J. Wang, *Phys. Rev. Lett.* **1990**, *64*, 2418.
[41] V. Mizeikis, S. Juodkazis, A. Marcinkevičius, S. Matsuo, H. Misawa, *J. Photochem. Photobiol. C Photochem. Rev.* **2001**, *2*, 35.
[42] J. Hou, M. Li, Y. Song, *Nano Today* **2018**, *22*, 132.
[43] R. V. Nair, R. Vijaya, *Prog. Quantum Electron.* **2010**, *34*, 89.
[44] P. Pawel, *Contemp. Phys.* **1983**, *24*, 25.
[45] M. Garzón et al., *Soft Matter* **2023**, *19*, 2360.
[46] Y. Takeoka, M. Watanabe, *Langmuir* **2003**, *19*, 9554.
[47] Y. Takeoka, T. Seki, *Langmuir* **2006**, *22*, 10223.
[48] H. E. Çamurlu et al., *Chem. Pap.* **2012**, *66*, 461.
[49] H. Saito, Y. Takeoka, M. Watanabe, *Chem. Commun.* **2003**, *3*, 2126.
[50] M. Li, D. Liu, H. Cheng, L. Peng, M. Zu, *Sci. Adv.* **2020**, *6*, 1.
[51] M. G. Abebe, G. Rosolen, E. Khousakoun, J. Odent, J. M. Raquez, S. Desprez, B. Maes, *Phys. Rev. Appl.* **2020**, *14*, 1.
[52] K. M. Lee et al., *Langmuir* **2019**, *19*, 5323.
[53] G. Mayonado, S. M. Mian, V. Robbiano, F. Cacialli. Investigation Of The Bragg-Snell Law In Photonic Crystals," 60–63. **2015**.
[54] W. Yuehui, Y. Xing, *Micro Nano Lett.* **2018**, *13*, 1349.
[55] Z. Sun, M. Gu, Y. Teng, X. Liu, B. Liu, J. Zhang, S. Huang, C. Ni, *Opt. Express* **2022**, *30*, 21324.
[56] M. Li, B. Bresson, F. Cousin, C. Fretigny, Y. Tran, *Langmuir* **2015**, *31*, 42, 11516.
[57] Y. Brasse, M. B. Müller, M. Karg, C. Kuttner, T. A. F. König, A. Fery, *ACS Appl. Mater. Interfaces* **2018**, *10*, 3133.
[58] R. Kitamura, L. Pilon, M. Jonasz, *Water Res.* **2007**, *46*, 8118.
[59] Y. Ji, Y. Jiang, H. Liu, L. Wang, D. Liu, C. Jiang, R. Fan, D. Chen, *Thin Solid Films* **2013**, *545*, 111.

[60] K. Ishikawa, H. Ogawa, S. Fujimura, *J. Appl. Phys.* **1999**, *85*, 4076.

SUPPORTING INFORMATION

Additional supporting information can be found online in the Supporting Information section at the end of this article.

How to cite this article:
M. G. Garzon Altamirano, M. G. Abebe, J. Lejeune, A. Cayla, B. Maes, J. Odent, J. M. Raquez, C. Campagne, E. Devaux, *J. Appl. Polym. Sci.* **2023**, *140*(27), e54004. https://doi.org/10.1002/app.54004